Van der Waals potential: an important complement to molecular electrostatic potential in studying intermolecular interactions

Tian Lu,[a],* Qinxue Chen[a]

[a] Beijing Kein Research Center for Natural Sciences, Beijing 100022, P. R. China (http://www.keinsci.com)

* Correspondence author. E-mail: sobereva@sina.com

ORCiD
Tian Lu: 0000-0002-1822-1229
Qinxue Chen: 0000-0003-0155-2387

Abstract: Electrostatic and van der Waals (vdW) interactions are two major components of intermolecular weak interactions. Electrostatic potential has been a very popular function in revealing electrostatic interaction between the system under study and other species, while the role of vdW potential is less recognized and has long been ignored. In this paper, we explicitly present definition of vdW potential, describe its practical implementation, and demonstrate its important value by visual analysis and comparing it with spatial distribution function obtained via molecular dynamics simulation. We hope this work can arouse researchers' attention to van der Waals potential and promote its application in practical studies of weak interaction. Calculation, visualization and quantitative analysis of the vdW potential have been supported by our freely available code Multiwfn (http://sobereva.com/multiwfn).

Keywords: van der Waals; electrostatic potential; Multiwfn; intermolecular interaction; adsorption

1. Introduction

It is widely accepted that intermolecular interaction can be divided into five components:[1] electrostatic interaction, exchange-repulsion, dispersion, polarization and charge-transfer, the latter two are less important for most cases. Usually, the electrostatic interaction plays a dominant role among all attractive components when the interacting molecules are polar, it is also able to control intermolecular relative orientation even if the molecules are nonpolar.[2] Due to the crucial role played by the electrostatic component, the electrostatic potential (ESP),[3, 4] which is a real space function in three-dimension space, is frequently studied in literatures[5-9] due to its usefulness in exhibiting possible electrostatic interaction between current system and external environment when detailed information of other molecules is unknown.

The exchange-repulsion interaction showing repulsive effect and the dispersion interaction showing attractive effect are collectively known as van der Waals (vdW) interaction, the role of vdW interaction should never been ignored. Near equilibrium geometry of a molecular cluster, the magnitude of exchange-repulsion is always significant; between two nonpolar molecules, the contribution from dispersion interaction to intermolecular attraction is even greater than that of electrostatic interaction, as shown in our recent study of cyclo[18]carbon dimer.[10]

In most molecular forcefields, the electrostatic interaction between two molecules (*e.g. K* and *L*) is simply evaluated based on atomic charges[11]

$$E_{K,L}^{\mathrm{els}} = \sum_{A}^{\mathrm{mol}\,K} \sum_{B}^{\mathrm{mol}\,L} \frac{q_A q_B}{|\mathbf{R}_A - \mathbf{R}_B|} \tag{1}$$

where $\mathbf{R}_A$ and $\mathbf{R}_B$ denote nuclear coordinates of atoms *A* and *B*, respectively, and *q* stands for atomic charge. Correspondingly, ESP of a molecule can be calculated as follows by simply assuming the acting object is a point charge located at $\mathbf{r}$

$$V^{\mathrm{els}}(\mathbf{r}) = \sum_{A} \frac{q_A}{|\mathbf{R}_A - \mathbf{r}|} \tag{2}$$

The vdW interaction energy between two atoms is usually evaluated in terms of Lennard-Jones 12-6 pair potential in below form[12]

$$\begin{aligned} E_{K,L}^{\mathrm{vdW}} &= \sum_{A}^{\mathrm{mol}\,K} \sum_{B}^{\mathrm{mol}\,K} \left(E_{AB}^{\mathrm{repul}} + E_{AB}^{\mathrm{disp}} \right) \\ &= \sum_{A}^{\mathrm{mol}\,K} \sum_{B}^{\mathrm{mol}\,K} \left[\varepsilon_{AB} \left(\frac{R_{AB}^0}{|\mathbf{R}_A - \mathbf{R}_B|} \right)^{12} - 2\varepsilon_{AB} \left(\frac{R_{AB}^0}{|\mathbf{R}_A - \mathbf{R}_B|} \right)^{6} \right] \end{aligned} \tag{3}$$

where the potential well ε and equilibrium distance R^0 (the position of the bottom of the interaction curve) are dependent of atom types. The two components of E^{vdW}, namely E^{repul} and E^{disp}, correspond to exchange-repulsion and dispersion interactions, respectively.

Following the spirit of ESP, we define vdW potential of a chemical system as follows

$$V^{\mathrm{vdW}}(\mathbf{r}) = V^{\mathrm{repul}}(\mathbf{r}) + V^{\mathrm{disp}}(\mathbf{r}) = \sum_{A} \varepsilon_{AB} \left(\frac{R_{AB}^0}{|\mathbf{R}_A - \mathbf{r}|} \right)^{12} + \sum_{A} \left[-2\varepsilon_{AB} \left(\frac{R_{AB}^0}{|\mathbf{R}_A - \mathbf{r}|} \right)^{6} \right] \tag{4}$$

The V^{repul} and V^{disp} denote exchange-repulsion and dispersion potentials, respectively. Clearly the

definition of vdW potential relies on the choice of atom *B*, which can be regarded as a probe atom. In addition, it should be noted that the vdW potential is related to forcefield, since vdW parameters in different forcefields are usually different.

Since ESP has important practical values in revealing electrostatic interaction between the molecule under study and external environment, it is naturally expected that vdW potential should also have some sort of capacity in revealing vdW interaction between a given system and other species, and thus behave as a complement to the ESP in the study of weak interactions. In the rest of this article, we will first describe how vdW potential is implemented in our wavefunction analysis code Multiwfn,[13] and then in Section 3 we will present a few examples of vdW potential to discuss its character and illustrate its value in practical applications, in the final section we summarize this article.

2. Implementation of van der Waals potential in Multiwfn

vdW potential analysis has been supported in Multiwfn since version 3.7, this code can be freely obtained at http://sobereva.com/multiwfn. In our implementation, the vdW parameters from UFF forcefield[14] are employed, because the elements supported by UFF almost cover the whole periodic table (H~Lr), and the parameters are only dependent of element, thus the assignment of atom types does not need to be explicitly considered. These advantages of UFF forcefield make vdW potential analysis easy to be employed for any kind of system. In principle, the vdW potential can also be calculated based on other forcefields such as GAFF,[15] however other forcefields are not taken into account since by comparing atomic vdW parameters we believe using other forcefield parameters instead of the UFF ones should not qualitatively change the analysis result. The ε_{AB} and R_{AB}^0 terms involved in the vdW potential are evaluated via geometric combination rule based on the atomic nonbond parameters defined in the UFF forcefield, that is

$$\varepsilon_{AB} = \sqrt{\varepsilon_A \varepsilon_B} \qquad R_{AB}^0 = \sqrt{R_A^0 R_B^0} \tag{5}$$

In Multiwfn, the element of probe atom is determined by "ivdwprobe" parameter in *settings.ini* file of Multiwfn. To perform vdW potential analysis, the input file only needs to record molecular structure, therefore many popular file formats can be used, such as .xyz, .pdb, .mol and .mol2. The grid data of vdW potential can be calculated by subfunction 6 of main function 20, the corresponding code is efficient and parallelized, calculation of grid data of V^{vdW}, V^{repul} and V^{disp} can be completed within one second even for system consisting of hundreds of atoms. The yielded grid data can be directly visualized as isosurface map or be exported as cube files. In addition, the basin analysis module of Multiwfn has capacity of searching global and all local minima and maxima of a real space function, via this function the minima of V^{vdW} can be rapidly located, the values at these points are useful in quantitatively comparing strength of vdW potential between different sites of the same system or between similar sites in different systems. The V^{vdW}, V^{repul} and V^{disp} also correspond to user-defined functions 92, 93 and 94 in Multiwfn, respectively. Since Multiwfn has powerful functions in visualizing any supported real space function, these potentials can be directly and easily plotted as curve map and various types of plane maps.

Interested readers are recommended to refer to Section 4.20.6 of Multiwfn manual, in which detailed instruction and examples of studying vdW potential are given.

3. Illustrative examples

In this part, we select a few molecules to exhibit their vdW potentials. Our purpose is not to very comprehensively demonstrate practical values and applications of this function, but to give readers an intuitive understanding of distribution characteristics of the vdW potential and to let readers know which information of chemical interest is conveyed by this function. Therefore, only relatively simple cases are taken into account, namely only noble gas elements are taken as probe atoms and the examined molecules are basically composed of carbon and hydrogen atoms, since molecular polarity in this situation is nearly negligible, and thus the interaction between the probe atom and the molecule under study is fully dominated by vdW interaction, while contribution of electrostatic component can be safely ignored.

Although Multiwfn is able to directly generate isosurface map for vdW potential, VMD 1.9.3 program[16] was employed to render some isosurface maps based on cube file exported by Multiwfn to gain better graphical effect. All plane maps were directly generated by Multiwfn. Geometries of all involved monomer structures except for cyclo[18]carbon have been optimized by Gaussian 16 A.03 program[17] at B3LYP/6-31G* level.[18, 19] The molecular dynamics (MD) simulation was realized by xtb 6.3 preview 2 code[20] based on GFN0-xTB[21] or GFN1-xTB[22] theory. The GFN-xTB series of theory can be regarded as a semi-empirical variant of density functional theory,[21] since it is quite efficient, we were able to conduct the MD simulation for a long time to ensure adequate sampling. GFN0-xTB is the cheapest and crudest version of GFN-xTB theory, the GFN1-xTB is evidently more accurate and robust than GFN0-xTB while the cost is increased by about one order of magnitude. The visualization and analysis of MD trajectories were realized by VMD 1.9.3.

3.1 7-helicene

First, we study vdW potential of 7-helicene, which is a molecule combined by seven six-membered carbon rings, its geometry is shown in Fig. 1. In this example, He is chosen as probe atom, the isosurface maps of corresponding vdW potential ($V_{\mathrm{He}}^{\mathrm{vdW}}$) are given in Fig 2.

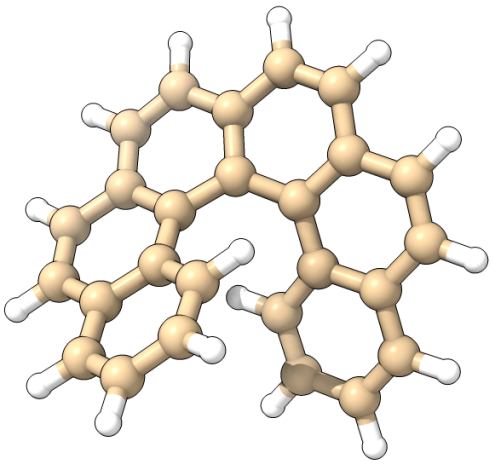

Fig. 1 Geometry of 7-helicene.

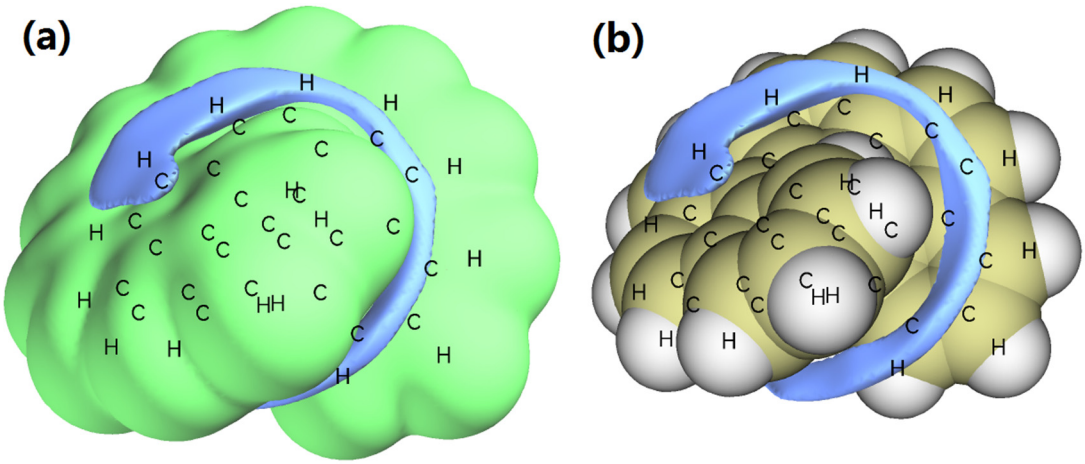

Fig. 2 0.5 kcal/mol isosurface of vdW potential of 7-helicene, He is chosen as probe atom. (a) Green and blue surfaces correspond to positive and negative parts, respectively (b) Only the negative part is shown.

In Fig. 2, the blue isosurface represents the region where $V_{\mathrm{He}}^{\mathrm{vdW}}$ is negative. In this region dispersion attraction effect surpasses exchange-repulsion effect, since the former and the latter have positive and negative contributions to the vdW potential, respectively. It is expected that the probe atom He (or more generally, small nonpolar molecules such as N_2) tends to be attracted to the blue region due to the driven force of dispersion attraction. The region close to the nuclei is fully enclosed by green isosurface, indicating that exchange-repulsion potential dominates the vdW potential in this area. It is easy to understand if a He atom is placed within the green isosurface, it must be repelled due to strong exchange-repulsion effect, this phenomenon is also known as steric hindrance.

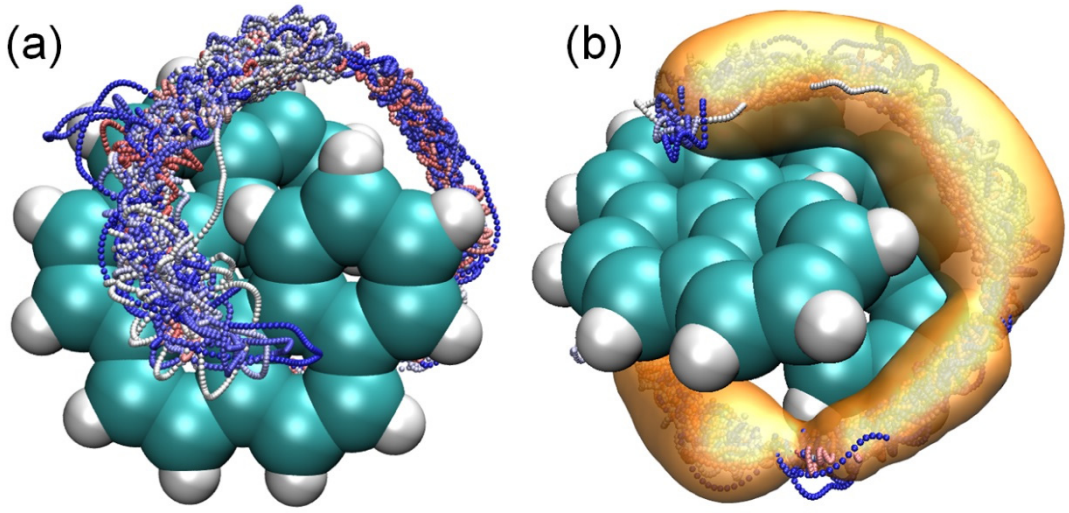

Fig. 3 MD simulation result of the complex composed of a He atom and 7-helicene at 10 K (a) Superposition of He atom in all MD frames, the trajectory is colored according to time step using blue-white-red color transition (b) Another view with an isosurface of spatial distribution function of the He atom during the MD simulation.

Can the map of $V_{\mathrm{He}}^{\mathrm{vdW}}$ be correlated with any practical observation? The answer is Yes. To

demonstrate this point, we carried out 2500 ps MD simulation for the complex composed of a 7-helicene molecule and a He atom via GFN0-xTB theory. The simulation temperature was maintained at 10 K by Berendsen thermostat,[23] we chose such a low temperature because the well depth between the He and the 7-helicene is shallow, at a higher temperature the He cannot be stably bounded by the vdW potential. The trajectory dumping frequency is set to be 50 fs, therefore totally 50000 frames were gathered from the simulation. The superposition map of the He in all MD frames is given in Fig. 3(a) and the trajectory is colored according to time step. It can be seen that the He atom repeatedly shuttles along the gap of the 7-helicene structure, the distribution of accumulated trajectory is quite similar to the negative isosurface of the $V_{\mathrm{He}}^{\mathrm{vdW}}$ (Fig. 2), demonstrating that vdW potential has certain ability to predict movement behavior of nonpolar small molecule around a host molecule.

In order to make the statistical distribution of the He atom during the MD simulation easier to examine, we also calculated spatial distribution function (SDF) via VolMap plugin of VMD, in which Gaussian broadening is employed to make this function smoother. An isosurface of SDF is shown in Fig. 3(b). By comparing this map with Fig. 2(b) it can be found that the shape of SDF is highly analogous to the dispersion dominated region of the $V_{\mathrm{He}}^{\mathrm{vdW}}$, well demonstrating that the vdW potential is able to reveal favorable physical adsorption zones (however, the prerequisite is that both the adsorbate and the local region of the adsorption sites are nearly nonpolar, otherwise electrostatic interaction will largely control the adsorption behavior, in this case one should investigate ESP prior to vdW potential).

3.2 Cyclo[18]carbon

The cyclo[18]carbon system was very extensively studied in our recent work,[10] it is a ring consisting of eighteen carbon atoms with point group of D_{9h}. The isosurface maps of vdW potentials of this system respectively using He, Ne, Ar and Xe as probe atom are given in Fig. 4; for clarity, only the negative part of the potential is shown, since usually only this part is of great chemical interest. The most negative points (global minima) of the vdW potentials are also plotted and the values are labelled, so that the potentials can be compared quantitatively. The geometry of cyclo[18]carbon was taken from Ref. [10].

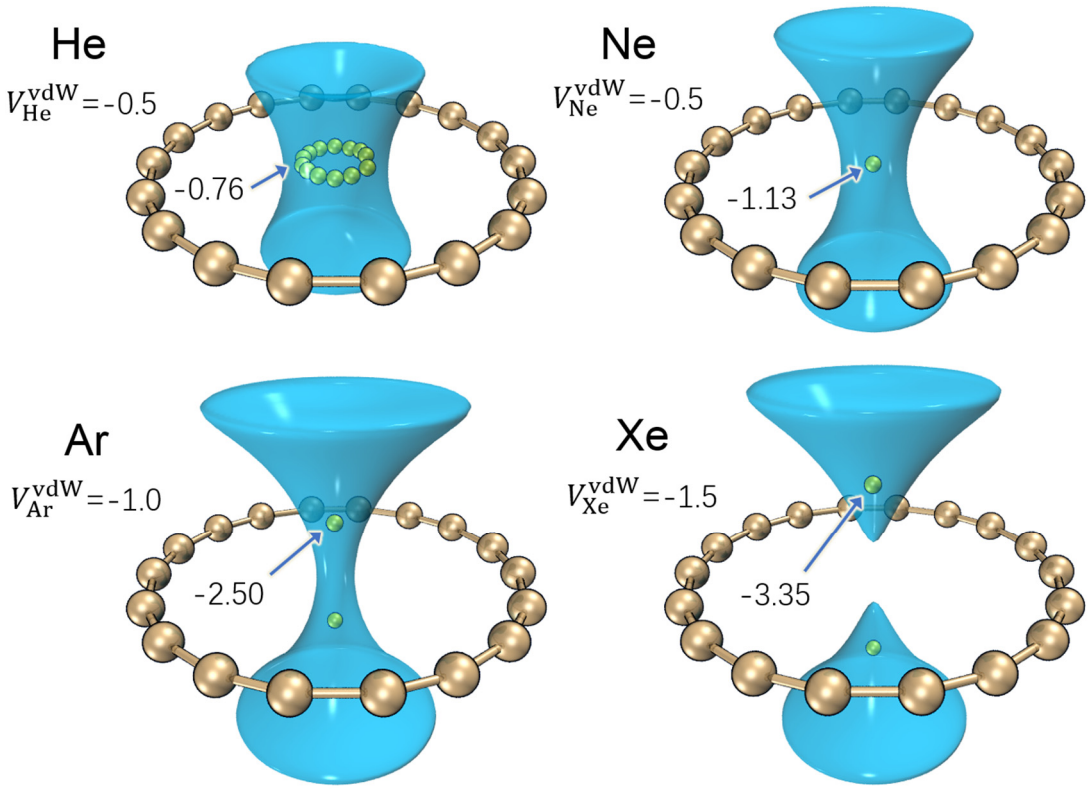

Fig. 4 Isosurface maps of vdW potential of cyclo[18]carbon using various probe atoms, only the negative part is shown. The isovalues of the isosurfaces are indicated. The small yellow spheres correspond to the most negative points. The isovalues are properly chosen for different cases so that the major distribution character of the potentials can be viewed clearly and compared easily. The units of the labelled numbers are all kcal/mol.

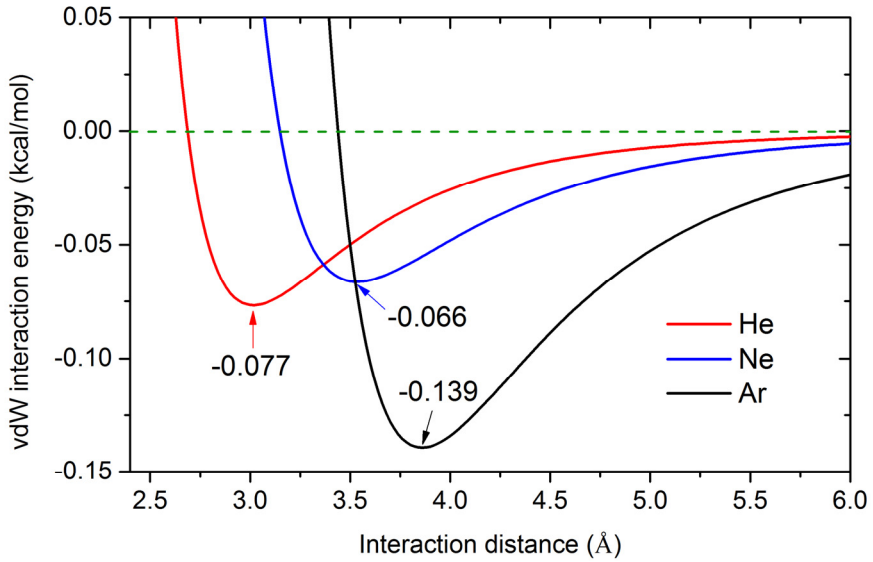

Fig. 5 vdW interaction curve between a carbon atom and various noble gas atoms. The minima of the curves are labelled. The intersections of the curves and the green dash line correspond to the positions where exchange-repulsion potential exactly equals to dispersion potential.

From Fig. 4 it can be seen that the shape and magnitude of negative part of vdW potential is quite sensitive to the choice of probe atom. Let us consider the four cases respectively:

(1) He as probe atom: Wide region around the center of the cyclo[18]carbon shows negative vdW potential. The most negative points are degenerate and form a ring, as shown by the small yellow spheres in Fig. 4. These minima have value of -0.76 kcal/mol, indicating that the binding energy between cyclo[18]carbon and a He atom due to vdW interaction can be at most 0.76 kcal/mol. It should be noted that this value should be crude and only qualitatively correct, since accuracy of UFF forcefield is very limited. More accurate vdW interaction energy can be obtained via other techniques such as high-order symmetry adapted perturbation theory (SAPT) theory.[1, 24-26]

(2) Ne as probe atom: In the inner region of the cyclo[18]carbon, the negative isosurface of the vdW potential is evidently thinner than the case when He is selected as the probe atom, this is because radius of Ne is larger than He, making the exchange-repulsion potential exceed the dispersion potential in broader region. This point can be clearly seen from the intersections between the vdW interaction curves and the green dash line in Fig. 5, which correspond to the positions where exchange-repulsion potential just equals to dispersion potential.

As shown in Fig. 4, there is only one minimum of $V_{\mathrm{Ne}}^{\mathrm{vdW}}$ at the center of the ring, whose value (-1.13 kcal/mol) is obviously more negative than when He is chosen as probe atom (-0.76 kcal/mol), this observation implies that Ne has stronger ability to bind to the cyclo[18]carbon. The source of this difference cannot be explained by well depths, since in the UFF forcefield the depth parameter of He (0.056 kcal/mol) is even larger than Ne (0.042 kcal/mol). The reason should be attributed to the collective effect of the 18 carbon atoms. According the vdW interaction curve between a carbon and a He or a Ne atom shown in Fig. 5, the equilibrium distance of the C-Ne curve appears much farther than the C-He curve, and its distance 3.54 Å is only marginally smaller than the radius of the cyclo[18]carbon (3.69 Å), this feature of vdW interaction potential happens to make the ring center of the cyclo[18]carbon be the global minimum of the $V_{\mathrm{Ne}}^{\mathrm{vdW}}$, and this is why its value -1.13 kcal/mol is about 18 times of the well depth of the C-Ne curve shown in Fig. 5 (-0.066 kcal/mol).

(3) Ar as probe atom: From Fig. 4 it can be seen that in this case the number of minima of vdW potential becomes two, they are symmetrically distributed on the upper and lower sides of the cyclo[18]carbon, and their values (-2.50 kcal/mol) are by far more negative than the previous two cases. This finding is entirely expected, since the depth parameter of Ar in UFF forcefield (0.185 kcal/mol) is more than three times higher than that of He and Ne, this point is also implicitly reflected by the vdW interaction curves shown in Fig. 5. The reason why there are two minima of $V_{\mathrm{Ar}}^{\mathrm{vdW}}$ rather than only one is also easy to understand: the equilibrium distance of the vdW interaction curve of C-Ar ($R_{\mathrm{C-Ar}}^{0}$=3.86 Å) is larger than the radius of the cyclo[18]carbon, therefore the global minima of the $V_{\mathrm{Ar}}^{\mathrm{vdW}}$ contributed by the 18 carbons must occur above and below the ring plane with value exactly equals to 18 times of the well depth of the C-Ar interaction curve (namely -0.139×18= -2.50 kcal/mol) and with distance to the carbons exactly equals to $R_{\mathrm{C-Ar}}^{0}$.

(4) Xe as probe atom: The value of minima of vdW potential in this case is even more negative than the case of Ar as probe atom due to deeper depth parameter of Xe (0.332 kcal/mol) in UFF forcefield. A noteworthy point of the $V_{\mathrm{Xe}}^{\mathrm{vdW}}$ is that the isosurface of -1.5 kcal/mol is dissected at the ring center, which implies that $V_{\mathrm{Xe}}^{\mathrm{vdW}}$ at ring center is not very negative or may even be positive, thus it is expected that Xe atom can hardly pass through the ring. This observation is clearly the direct consequence of the fairly large vdW radius of Xe.

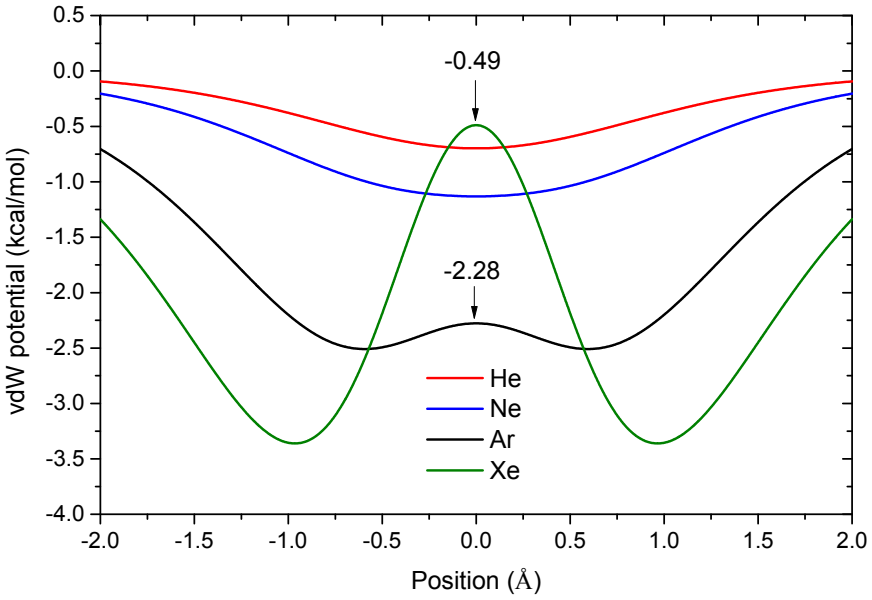

Fig. 6 Variation of vdW potential perpendicular to cyclo[18]carbon plane with ring center as the origin of the map. Four probe atoms are taken into account.

Fig. 6 displays variation of vdW potential perpendicular to the ring plane of the cyclo[18]carbon with the ring center as origin. It can be clearly seen that the vdW potentials with Ar and Xe as probe atom ($V_{\mathrm{Ar}}^{\mathrm{vdW}}$ and $V_{\mathrm{Xe}}^{\mathrm{vdW}}$) show double well characteristics due to the reason explained earlier, while for the other cases the potential curve only has one minimum. Besides, as shown by the green curve in Fig. 6, the $V_{\mathrm{Xe}}^{\mathrm{vdW}}$ in fact is slightly negative around the center of the ring, the maximum point exactly locates at the ring center and the value is -0.49 kcal/mol. Despite that dispersion attractive effect surpasses exchange-repulsive effect at the ring center, since the gradient of the $V_{\mathrm{Xe}}^{\mathrm{vdW}}$ on both sides of the peak is quite large, it is very difficult for Xe atom to pass through the ring center due to the strong repulsion force. In contrast, Ar atom should be able to freely shuttle back and forth on both sides of the cyclo[18]carbon, since the barrier represented by the $V_{\mathrm{Ar}}^{\mathrm{vdW}}$ curve is negligible, which is merely 0.22 kcal/mol (corresponding to the difference between the -2.28 labelled on Fig. 6 and the -2.50 labelled on Fig. 4).

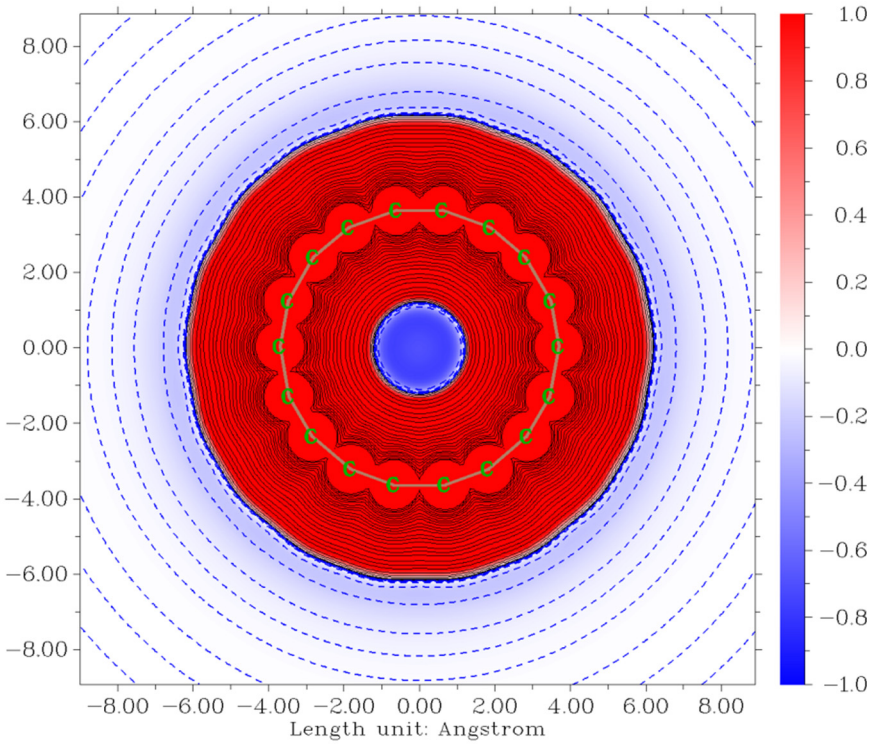

Fig. 7 Plane map of vdW potential with He as probe atom on the ring plane of cyclo[18]carbon. The positive part (colored by red) and negative part (colored by blue) correspond to the regions dominated by exchange-repulsion potential and dispersion potential, respectively. The unit of the potential is kcal/mol.

To present a more complete picture about the vdW potential, we plotted color-filled map with contour lines for $V_{\mathrm{He}}^{\mathrm{vdW}}$ of the cyclo[18]carbon, as shown in Fig. 7. This map shows that the region near nuclei is fully dominated by exchange-repulsion potential and thus the $V_{\mathrm{He}}^{\mathrm{vdW}}$ is considerably positive. The most negative zone occurs around the ring center, mainly because all the 18 atoms have prominent contribution to this region. The $V_{\mathrm{He}}^{\mathrm{vdW}}$ is also negative at peripheral region of the ring, but the magnitude is fairly small compared to the ring center, this is because vdW potential decays rapidly as interaction distance increases, in this system only a few atoms can have detectable contribution to the vdW potential of a point located at peripheral region of the ring. In order to demonstrate this, we built a complex consisting of a cyclo[18]carbon and a He atom 3.0 Å away from it, the atom pair contributions to the vdW interaction are shown in Fig. 8. From this figure it is seen that only the four carbon atoms closest to the He atom have detectable contribution, while the contributions from more distant atoms are fully negligible.

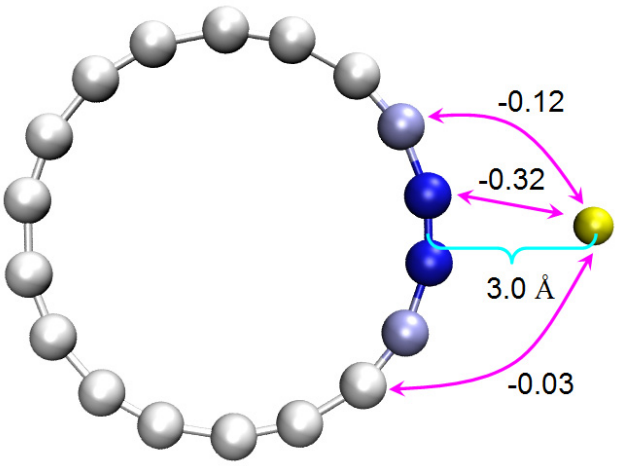

Fig. 8 Contribution of atom pairs to vdW interaction energy between cyclo[18]carbon and a He atom placed at peripheral region of the ring. For intuitive comparison, the carbon atoms are colored according to their contributions to the total interaction energy, which is calculated to be -0.95 kJ/mol (-0.23 kcal/mol) at UFF forcefield level. The unit of the labelled energies are kJ/mol.

Overall, the vdW potential substantially reveals that the most favorable adsorption site for small nonpolar molecules like H_2, N_2 and CH_4 on the cyclo[18]carbon should be the region close to the ring center; while at peripheral area of the ring, the small molecules can only be very loosely bound. However, this statement may not be suitable for polar molecules, since as shown in Ref. [10], the ESP distribution over the vdW surface of the cyclo[18]carbon is evidently uneven, therefore electrostatic interaction may play a more crucial role than vdW interaction in determination of preferential adsorption sites.

3.3 Porphyrin

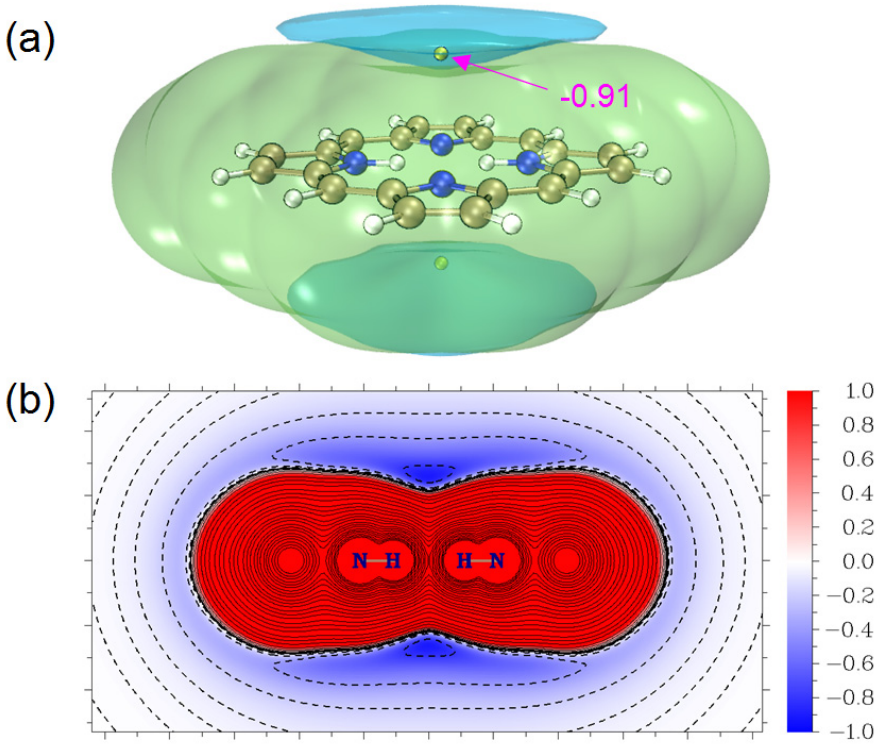

Fig. 9 vdW potential of porphyrin with Ne as probe atom. (a) Isosurfaces corresponding to 0.6 kcal/mol, both positive (green) and negative (blue) parts are shown, the yellow spheres highlight the minima positions, and the value is labelled in kcal/mol (b) Color-filled map with contour lines on the plane perpendicular to the molecule and along the two N-H bonds. The color scale is in kcal/mol.

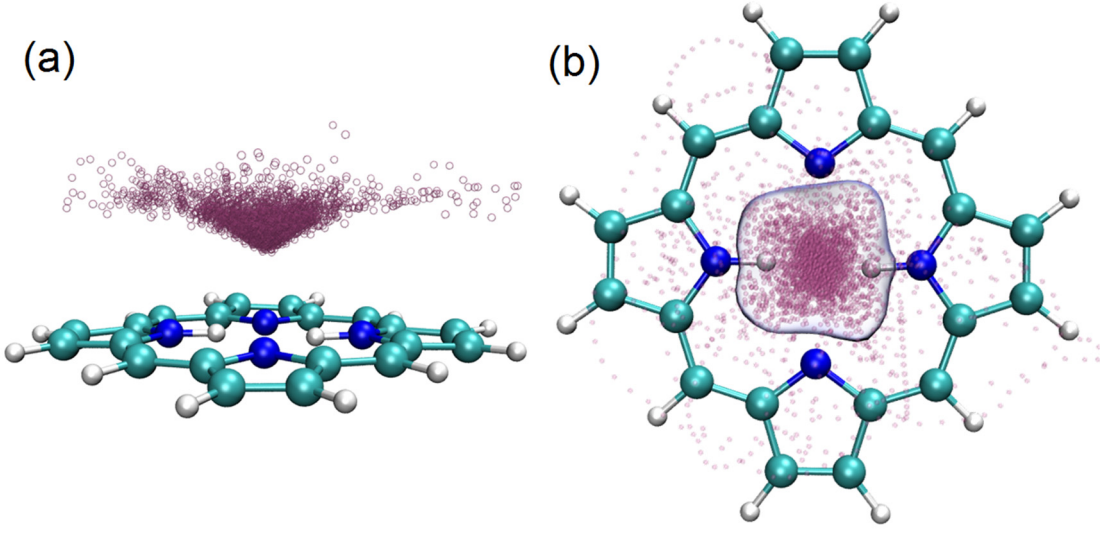

Fig. 10 MD simulation result of the complex composed of a porphyrin molecule and a Ne atom, two side views are given. These figures exhibit superposition of Ne atom in all MD frames. For easier inspection, an isosurface of spatial distribution function of Ne is drawn as transparent blue isosurface in (b).

Next, we study characteristics of vdW potential for porphyrin, which is a ring-like molecule with more complicated structure than the cyclo[18]carbon. For simplicity, only Ne is chosen as

probe atom. The isosurface map and color-filled plane map of the $V_{\mathrm{Ne}}^{\mathrm{vdW}}$ of this system are shown in Fig. 9. Furthermore, we conducted 1000 ps MD simulation using GFN1-xTB theory for a complex composed of a porphyrin molecule and a Ne atom, low temperature (about 40 K) was maintained via thermostat because higher temperature is found to dissociate this complex. During the simulation, a spherical restraint potential was applied to avoid the Ne occasionally escaping due to excess thermal motion. The superposition map of the Ne atom in the 4000 frames produced by the MD simulation is given in Fig. 10.

From Figs. 9 and 10 it can be seen that since the pore at the center of the porphyrin is negligible, even the very small Ne atom is unable to pass through the molecule, therefore during the entire MD process the Ne only occurs on one side. The most negative regions of the $V_{\mathrm{Ne}}^{\mathrm{vdW}}$ appear above and below the ring center, the value at the corresponding minimum is found to be -0.91 kcal/mol, which is slightly smaller than the cyclo[18]carbon case we discussed above, mostly because porphyrin (and other common organic molecules) does not have so ideal arrangement of heavy atoms like the cyclo[18]carbon.

By comparing Figs. 9 and 10, we noticed that both the vdW potential isosurface and the region where the Ne visits most frequently during the MD simulation show cone shape, and their distributions look quite similar, this observation again manifests that the vdW potential is able to nicely portray the preferential appearance region of particles interacting with the current system in actual situation, at least when temperature is sufficiently low and electrostatic interaction plays an insignificant role.

3.4 Carbon nanotube fragment

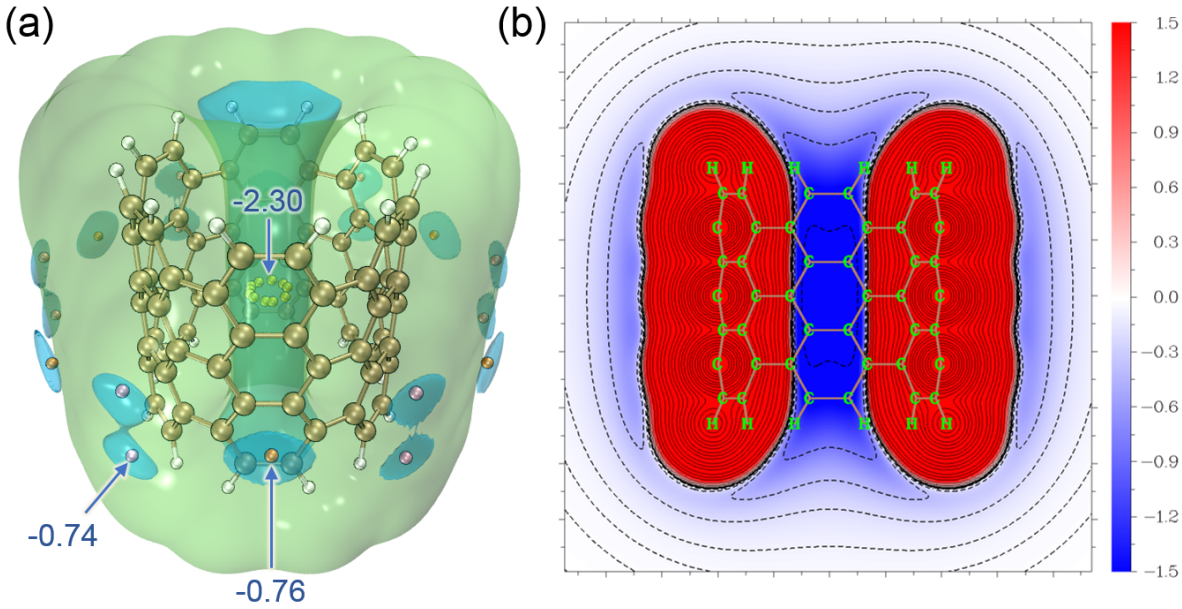

Fig. 11 vdW potential with Ne as probe atom of a fragment of carbon nanotube of (6,6) chiral index. (a) Isosurface map with isovalue of 0.7 (green) and -0.7 (blue) kcal/mol. Three kinds of minima are respectively represented as yellow, orange and pink spheres, and the vdW potentials at these points are labelled on the figure in kcal/mol. (b) vdW potential in a cutting plane of the nanotube fragment. Contour lines of positive and negative parts are in solid and dash style, respectively. The color scale is in kcal/mol.

The final example is a fragment of carbon nanotube of (6,6) chiral index, the boundary has been saturated by hydrogens. Isosurface map and plane map of vdW potential of this system are given in Fig. 11, Ne is chosen as probe atom. In Fig. 11(a), not only global minima of the $V_{\mathrm{Ne}}^{\mathrm{vdW}}$ are highlighted by yellow spheres, but also two kinds of local minima are drawn as pink and orange spheres, respectively. The Fig. 11(a) shows that Ne atom feels strongest van der Waals attraction inside the tube, at the central region of the nanotube fragment the $V_{\mathrm{Ne}}^{\mathrm{vdW}}$ can reach as high as -2.30 kcal/mol, which is more than double of the cyclo[18]carbon case. The main reason is that this system has a compact three-dimensional structure, so there are many carbon atoms that have strong dispersion attraction to a particle located at the central region of the system. In the outer region of the tube the $V_{\mathrm{Ne}}^{\mathrm{vdW}}$ is also negative, however the value is at most -0.76 kcal/mol, which is much weaker than the counterpart in the inner region. From the plane map in Fig. 11(b), this distribution characteristic of $V_{\mathrm{Ne}}^{\mathrm{vdW}}$ can be inspected more clearly. The vdW potential presented in this example shows that carbon nanotubes have a strong tendency to adsorb small molecules to its inside.

4. Summary

Electrostatic and dispersion interactions are two major components of intermolecular interaction. Electrostatic potential (ESP) has been a well-known tool in estimation of electrostatic interaction between a chemical system and other species. By following the idea of ESP, in this work we explicitly defined vdW potential, which can be viewed as a complement to ESP in investigating intermolecular interactions as it can intuitively exhibit vdW interaction between a molecule and a probe atom. We also presented four examples to show distribution characteristics of the vdW potential and compared it with particle distribution resulting from MD simulations. Though the examples are relatively simple, the important value of the vdW potential in revealing the preferential sites controlled by vdW interaction has already been well demonstrated, and meantime our implementation of the vdW potential based on UFF forcefield parameters is justified. Since vdW potential has been supported in our analysis code Multiwfn and only geometry information is needed as input, it is expected that the vdW potential may become one of standard analysis methods in studying physical adsorption, explaining stability and structure of molecular cluster and so on. However, care should be taken that if the interacting molecules show prominent polar character, then usually electrostatic interaction rather than vdW interaction dominates the intermolecular binding, in this case overinterpretation of vdW potential should be avoided, otherwise the conclusion may be misleading.

References

1. S. Emamian; T. Lu; H. Kruse; H. Emamian. Exploring Nature and Predicting Strength of Hydrogen Bonds: A Correlation Analysis Between Atoms-in-Molecules Descriptors, Binding Energies, and Energy Components of Symmetry-Adapted Perturbation Theory. *J. Comput. Chem.*, **40**, 2868 (2019). DOI: 10.1002/jcc.26068.

2. T. Lu; F. Chen. Revealing the nature of intermolecular interaction and configurational preference

of the nonpolar molecular dimers (H2)2, (N2)2, and (H2)(N2). *J. Mol. Model.*, **19**, 5387 (2013). DOI: 10.1007/s00894-013-2034-2.

3. T. Lu; F. Chen. Quantitative analysis of molecular surface based on improved Marching Tetrahedra algorithm. *J. Mol. Graph. Model.*, **38**, 314 (2012). DOI: 10.1016/j.jmgm.2012.07.004.

4. J. S. Murray; P. Politzer. The electrostatic potential: an overview. *WIREs: Comp. Mol. Sci.*, **1**, 153 (2011). DOI: 10.1002/wcms.19.

5. R. Fu; T. Lu; F. Chen. Comparison of the Methods for Predicting the Reactive Site of Electrophilic Substitution Reaction. *Acta Phys. -Chim. Sin.*, **30**, 628 (2014).

6. J.-L. Jin; H.-B. Li; T. Lu; Y.-A. Duan; Y. Geng; Y. Wu; Z.-M. Su. Density functional studies on photophysical properties and chemical reactivities of the triarylboranes: effect of the constraint of planarity. *J. Mol. Model.*, **19**, 3437 (2013). DOI: 10.1007/s00894-013-1845-5.

7. S. Manzetti; T. Lu; H. Behzadi; M. D. Estrafili; H.-L. Thi Le; H. Vach. Intriguing properties of unusual silicon nanocrystals. *RSC Adv.*, **5**, 78192 (2015). DOI: 10.1039/C5RA17148B.

8. T. Lu; S. Manzetti. Wavefunction and reactivity study of benzo[a]pyrene diol epoxide and its enantiomeric forms. *Struct. Chem.*, **25**, 1521 (2014). DOI: 10.1007/s11224-014-0430-6.

9. S. Manzetti; T. Lu. The geometry and electronic structure of Aristolochic acid: possible implications for a frozen resonance. *J. Phys. Org. Chem.*, **26**, 473 (2013). DOI: 10.1002/poc.3111.

10. T. Lu; Q. Chen; Z. Liu. A thorough theoretical exploration of intriguing characteristics of cyclo[18]carbon: Geometry, bonding nature, aromaticity, weak interaction, reactivity, excited states, vibrations, molecular dynamics and various molecular properties. *ChemRxiv* (2019). DOI: 10.26434/chemrxiv.11320130.

11. T. Lu; F. Chen. Comparison of Computational Methods for Atomic Charges. *Acta Phys. -Chim. Sin.*, **28**, 1 (2012). DOI: 10.3866/PKU.WHXB2012281.

12. A. R. Leach. *Molecular modelling Principles and applications*. 2 ed.; Pearson Education: Essex, 2001.

13. T. Lu; F. Chen. Multiwfn: A Multifunctional Wavefunction Analyzer. *J. Comput. Chem.*, **33**, 580 (2012). DOI: 10.1002/jcc.22885.

14. A. K. Rappe; C. J. Casewit; K. S. Colwell; W. A. Goddard; W. M. Skiff. UFF, a full periodic table force field for molecular mechanics and molecular dynamics simulations. *J. Am. Chem. Soc.*, **114**, 10024 (1992). DOI: 10.1021/ja00051a040.

15. J. Wang; R. M. Wolf; J. W. Caldwell; P. A. Kollman; D. A. Case. Development and testing of a general amber force field. *J. Comput. Chem.*, **25**, 1157 (2004). DOI: 10.1002/jcc.20035.

16. W. Humphrey; A. Dalke; K. Schulten. VMD: Visual molecular dynamics. *J. Mol. Graph.*, **14**, 33 (1996). DOI: 10.1016/0263-7855(96)00018-5.

17. M. J. Frisch; G. W. Trucks; H. B. Schlegel; G. E. Scuseria; M. A. Robb; J. R. Cheeseman; G. Scalmani; V. Barone; G. A. Petersson; H. Nakatsuji; X. Li; M. Caricato; A. V. Marenich; J. Bloino; B. G. Janesko; R. Gomperts; B. Mennucci; H. P. Hratchian; J. V. Ortiz; A. F. Izmaylov; J. L. Sonnenberg; Williams; F. Ding; F. Lipparini; F. Egidi; J. Goings; B. Peng; A. Petrone; T. Henderson; D. Ranasinghe; V. G. Zakrzewski; J. Gao; N. Rega; G. Zheng; W. Liang; M. Hada; M. Ehara; K. Toyota; R. Fukuda; J. Hasegawa; M. Ishida; T. Nakajima; Y. Honda; O. Kitao; H. Nakai; T. Vreven; K. Throssell; J. A. Montgomery Jr.; J. E. Peralta; F. Ogliaro; M. J. Bearpark; J. J. Heyd; E. N. Brothers; K. N. Kudin; V. N. Staroverov; T. A. Keith; R. Kobayashi; J. Normand; K. Raghavachari; A. P. Rendell; J. C. Burant; S. S. Iyengar; J. Tomasi; M. Cossi; J. M. Millam; M. Klene; C. Adamo; R. Cammi; J. W. Ochterski; R. L. Martin; K. Morokuma; O. Farkas; J. B. Foresman; D. J. Fox. *Gaussian 16 A.03*, Wallingford, CT, 2016.

18. P. C. Hariharan; J. A. Pople. The influence of polarization functions on molecular orbital hydrogenation energies. *Theor. Chem. Acc.*, **28**, 213 (1973).

19. P. J. Stephens; F. J. Devlin; C. F. Chabalowski; M. J. Frisch. Ab Initio Calculation of Vibrational Absorption and Circular Dichroism Spectra Using Density Functional Force Fields. *J. Phys. Chem.*, **98**, 11623 (1994). DOI: 10.1021/j100096a001.

20. Stefan Grimme, et al., xtb program: https://github.com/grimme-lab/xtb/ (accessed on Apr 12, 2020).

21. P. Pracht; E. Caldeweyher; S. Ehlert; S. Grimme. A Robust Non-Self-Consistent Tight-Binding Quantum Chemistry Method for large Molecules. *ChemRxiv* (2019). DOI: 10.26434/chemrxiv.8326202.v1.

22. S. Grimme; C. Bannwarth; P. Shushkov. A Robust and Accurate Tight-Binding Quantum Chemical Method for Structures, Vibrational Frequencies, and Noncovalent Interactions of Large Molecular Systems Parametrized for All spd-Block Elements (Z = 1–86). *J. Chem. Theory Comput.*, **13**, 1989 (2017). DOI: 10.1021/acs.jctc.7b00118.

23. H. J. C. Berendsen; J. P. M. Postma; W. F. van Gunsteren; A. DiNola; J. R. Haak. Molecular dynamics with coupling to an external bath. *J. Chem. Phys.*, **81**, 3684 (1984). DOI: 10.1063/1.448118.

24. T. M. Parker; L. A. Burns; R. M. Parrish; A. G. Ryno; C. D. Sherrill. Levels of symmetry adapted perturbation theory (SAPT). I. Efficiency and performance for interaction energies. *J. Chem. Phys.*, **140**, 094106 (2014). DOI: 10.1063/1.4867135.

25. K. Szalewicz. Symmetry-adapted perturbation theory of intermolecular forces. *WIREs: Comp. Mol. Sci.*, **2**, 254 (2012). DOI: 10.1002/wcms.86.

26. Y. Jiao; Y. Liu; W. Zhao; Z. Wang; X. Ding; H. Liu; T. Lu. Theoretical study on the interactions of halogen-bonds and pnicogen-bonds in phosphine derivatives with Br2, BrCl, and BrF. *Int. J. Quantum Chem.*, **117**, e25443 (2017). DOI: 10.1002/qua.25443.